

**Mode-specific multi-channel dynamics of the  $F^- + CHD_2Cl$  reaction on a global ab initio potential energy surface**

István Szabó and Gábor Czakó

Citation: *The Journal of Chemical Physics* **145**, 134303 (2016); doi: 10.1063/1.4963664

View online: <http://dx.doi.org/10.1063/1.4963664>

View Table of Contents: <http://scitation.aip.org/content/aip/journal/jcp/145/13?ver=pdfcov>

Published by the **AIP Publishing**

---

**Articles you may be interested in**

**Communication: Mode specific quantum dynamics of the  $F + CHD_3 \rightarrow HF + CD_3$  reaction**

*J. Chem. Phys.* **144**, 171101 (2016); 10.1063/1.4948547

**Mode specificity in the  $OH + CHD_3$  reaction: Reduced-dimensional quantum and quasi-classical studies on an ab initio based full-dimensional potential energy surface**

*J. Chem. Phys.* **144**, 164303 (2016); 10.1063/1.4947252

**A full-dimensional quantum dynamics study of the mode specificity in the  $H + HOD$  abstraction reaction**

*J. Chem. Phys.* **142**, 064314 (2015); 10.1063/1.4907918

**Coupled potential energy surface for the  $F(2P) + CH_4 \rightarrow HF + CH_3$  entrance channel and quantum dynamics of the  $CH_4 \cdot F^-$  photodetachment**

*J. Chem. Phys.* **139**, 014309 (2013); 10.1063/1.4812251

**Quasiclassical trajectory calculations of correlated product distributions for the  $F + CHD_3$  ( $v_1 = 0, 1$ ) reactions using an ab initio potential energy surface**

*J. Chem. Phys.* **131**, 244302 (2009); 10.1063/1.3276633

---



**NEW Special Topic Sections**

**NOW ONLINE**  
Lithium Niobate Properties and Applications:  
Reviews of Emerging Trends

**AIP** | Applied Physics  
Reviews

# Mode-specific multi-channel dynamics of the $F^- + CHD_2Cl$ reaction on a global *ab initio* potential energy surface

István Szabó<sup>a)</sup> and Gábor Czako<sup>b)</sup>

Department of Physical Chemistry and Materials Science, Institute of Chemistry, University of Szeged, Rerrich Béla tér 1, Szeged H-6720, Hungary

(Received 10 August 2016; accepted 14 September 2016; published online 3 October 2016)

We report a detailed quasiclassical trajectory study for the dynamics of the ground-state and CH/CD stretching-excited  $F^- + CHD_2Cl(v_{CH/CD} = 0, 1) \rightarrow Cl^- + CHD_2F$ ,  $HF + CD_2Cl^-$ , and  $DF + CHDCl^-$   $S_N2$ , proton-, and deuteron-abstraction reactions using a full-dimensional global *ab initio* analytical potential energy surface. The simulations show that (a)  $CHD_2Cl(v_{CH/CD} = 1)$ , especially for  $v_{CH} = 1$ , maintains its mode-specific excited character prior to interaction, (b) the  $S_N2$  reaction is vibrationally mode-specific, (c) double inversion can occur and is enhanced upon CH/CD stretching excitations, (d) in the abstraction reactions the HF channel is preferred and the  $v_{CH/CD} = 1$  excitations significantly promote the HF/DF channels, (e) back-side rebound, back-side stripping, and front-side stripping are the dominant direct abstraction mechanisms based on correlated scattering- and attack-angle distributions, (f) the exact classical vibrational energy-based Gaussian binning (1GB) provides realistic mode-specific polyatomic product state distributions, (g) in the abstraction reactions CH and CD stretchings are not pure spectator modes and mainly ground-state products are produced, thus most of the initial energy transfers into product translation, and (h) the HF and DF product molecules are rotationally cold without any significant dependence on the reactant's and HF/DF vibrational states. *Published by AIP Publishing.* [<http://dx.doi.org/10.1063/1.4963664>]

## I. INTRODUCTION

The bimolecular nucleophilic substitution ( $S_N2$ ) is one of the most important reaction classes in organic and bio-organic chemistry. A stereo-specific optical-inversion mechanism of the  $S_N2$  reactions was discovered experimentally by Walden more than a hundred years ago.<sup>1</sup> After the early discovery, it took about 40 yr to explain its atomistic mechanism as discussed by Ingold in 1953.<sup>2</sup> Nowadays, Walden inversion is a well-known textbook example of the mechanism of  $S_N2$  reactions. However, recent theoretical and experimental studies<sup>3–5</sup> showed that  $S_N2$  reactions are “not so simple”<sup>6</sup> as highlighted by Xie and Hase in 2016.<sup>7</sup> Walden inversion can occur via direct rebound, direct stripping, and indirect pathways involving complex formations or roundabout.<sup>8–10</sup> Furthermore, retention mechanisms, such as the front-side attack<sup>11–13,4</sup> and the recently discovered double inversion<sup>4</sup> (see Figure 1), also exist. Despite the many known reaction mechanisms, the deeper, atomic-level understanding of the complex dynamics of  $S_N2$  reactions still requires further experimental and theoretical investigations.

Direct dynamics simulations, which compute the potential energies and gradients on-the-fly, have played a key role in uncovering the atomic-level pathways of  $S_N2$  reactions.<sup>3,8,10,14–16</sup> Recently, we developed the first high-level *ab initio*-based global analytical potential energy surfaces (PESs) for the  $F^- + CH_3Y$  [ $Y = F$  and  $Cl$ ] reactions,<sup>9,4,17</sup>

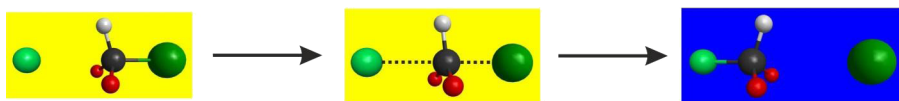
which have allowed efficient dynamical investigations using either the quasiclassical trajectory (QCT)<sup>4,5,9,17,18</sup> or reduced-dimensional quantum<sup>19</sup> methods. Using analytical PESs, one can compute millions of trajectories which provide unprecedented statistical accuracy for  $S_N2$  simulations and may reveal novel reaction mechanisms. Indeed, in 2015 we found a double-inversion pathway for the  $F^- + CH_3Cl$   $S_N2$  reaction, in which a proton-abstraction induced inversion followed by a second inversion via the usual central transition state results in overall retention.<sup>4</sup> Furthermore, in the case of the  $F^- + CH_3F$  reaction, our QCT simulations showed that front-side attack may become a dominant  $S_N2$  mechanism at very high collision energies.<sup>17</sup> As double inversion is induced by a proton abstraction, the proton transfer channel is especially interesting in the ion-molecule reactions. The analytical PES of the  $F^- + CH_3Cl$  reaction describes the proton-abstraction channel beside the above-mentioned  $S_N2$  pathways; thus, we can efficiently study the competing reaction channels and mechanisms.

In this study, we report QCT computations for the  $F^- + CHD_2Cl$  reaction, focusing on the  $Cl^- + CHD_2F$ ,  $HF + CD_2Cl^-$ , and  $DF + CHDCl^-$  product channels. The simulations may reveal interesting isotope effects and provide insight into the mechanisms of the proton/deuteron-transfer and double-inversion pathways. We are particularly interested in the role of the proton abstraction induced inversion in the double-inversion process and the partially deuterated reactant may provide additional insight by showing the mass effects on the mechanism if we manage to distinguish between the proton- and deuteron-induced inversions as shown in Fig. 1. Furthermore, we study the effects of the CH and

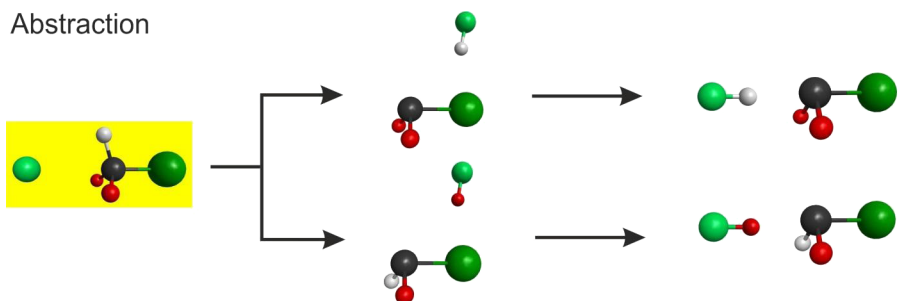
<sup>a)</sup>Present address: Department of Chemistry, King's College London, London SE1 1DB, United Kingdom.

<sup>b)</sup>Author to whom correspondence should be addressed. Electronic mail: gczako@chem.u-szeged.hu.

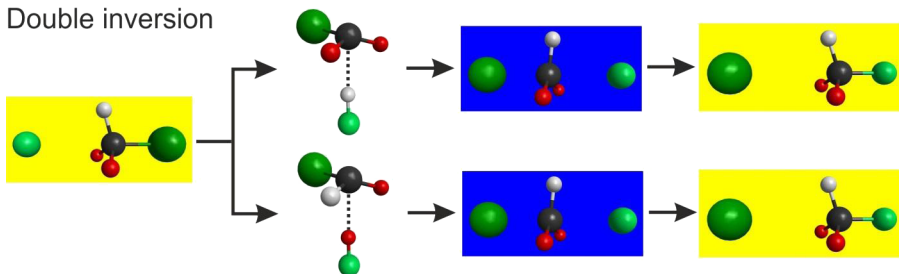
## Back-side attack



## Abstraction



## Double inversion



## Front-side attack

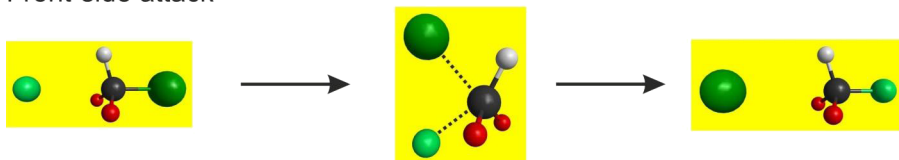


FIG. 1. Different channels and mechanisms of the  $F^- + CHD_2Cl$  reaction. Blue background denotes an inverted configuration relative to that of the reactant (yellow).

CD stretching excitations, which are expected to promote the corresponding abstraction channel as well as the double inversion. Utilizing our mode-specific product analysis and binning techniques,<sup>20,21</sup> we can follow the energy flow along the reaction coordinate from reactants to products. The mode-specific vibrational distributions of the polyatomic product molecules and ions may provide information about vibrational adiabaticity and test the utility of the one-dimensional Gaussian binning (1GB)<sup>20–22</sup> approach.

In Section II, we provide the methodological and computational details focusing on the vibrational mode-specific polyatomic product analysis and the different implementations of the 1GB approach. The QCT results on the inversion and retention pathways of the  $S_N2$  channel, proton and deuterium abstraction, and mode-specific energy transfer are described and discussed in Section III. The paper ends with summary and conclusions in Section IV.

## II. METHODS

### A. Computational details

The QCT computations are performed for the  $F^- + CHD_2Cl$  reaction employing our full-dimensional analytical *ab initio* PES developed for the  $F^- + CH_3Cl$  reaction in 2015.<sup>4</sup> The harmonic vibrational ground-state ( $v = 0$ ) and the stretching-excited states ( $v_{CH}(a') = 1$ ,  $v_{CD}(a') = 1$ , and

$v_{CD}(a'') = 1$ ) of the polyatomic reactant are prepared by standard normal mode sampling.<sup>23</sup> The initial rotational angular momentum of  $CHD_2Cl$  is set to zero by modifying the initial velocities.<sup>23</sup>

The initial orientation of  $CHD_2Cl$  is randomly selected and the distance of the reactants is  $\sqrt{x^2 + b^2}$ , where  $b$  is the impact parameter scanned with a step size of  $\Delta b$  from 0 to  $b_{max}$ , which is the maximum value of  $b$ , where any reactive event can occur. The settings for  $x$ ,  $\Delta b$ , and  $b_{max}$  values at each collision energy ( $E_{coll}$ ) are shown in Table I. Trajectories are run at  $E_{coll} = 1, 2, 4, 7, 10, 15, 20, 30, 40, 50$ , and 60 kcal/mol. At each  $b$ , 5000 trajectories are computed, except at  $E_{coll} = 50$  kcal/mol, where 25 000 trajectories are run at each  $b$  in order to get improved statistics for the correlated differential cross sections and mode-specific product state distributions, resulting in more than  $6 \times 10^6$  trajectories in this study. The trajectories are propagated using the velocity Verlet algorithm with a 0.0726 fs (3 a.u. of time) time step allowing a maximum of 4 500 000 steps (327 ps), but most of the trajectories finish much faster within a few picoseconds. The trajectories are stopped when the maximum of the actual inter-atomic distances is 1 bohr larger than the initial one. In case of the highly exothermic  $F^- + CHD_2Cl \rightarrow CHD_2F + Cl^-$  substitution reaction, the product zero-point energy (ZPE) violation is not a concern. However, for the substantially endothermic  $F^- + CHD_2Cl \rightarrow CD_2Cl^- + HF$  and  $CHDCl^- + DF$  abstraction reactions, the ZPE violation of the products is not

TABLE I. Settings for the initial distance of the reactants and impact parameter scans (in bohr) and the total number of trajectories at each collision energy ( $E_{\text{coll}}$  in kcal/mol).<sup>a</sup>

$E_{\text{coll}}$	$x$	$\Delta b$	$b_{\text{max}}^b$	$N_{\text{traj}}^b$
1	30	1.0	25	130 000
2	25	1.0	21	110 000
4	20	0.5	18	185 000
7	20	0.5	15	155 000
10	20	0.5	13	135 000
15	20	0.5	11	115 000
20	20	0.5	9	95 000
30	20	0.5	9	95 000
40	20	0.5	8	85 000
50	20	0.5	7	375 000 <sup>c</sup>
60	20	0.5	7	75 000

<sup>a</sup>The initial distance of the reactants is  $(x^2 + b^2)^{1/2}$ , where  $b = 0, \Delta b, 2\Delta b, \dots, b_{\text{max}}$  and  $N_{\text{traj}} = (b_{\text{max}}/\Delta b + 1) \times 5000$ .

<sup>b</sup> $b_{\text{max}}$  and  $N_{\text{traj}}$  slightly vary for the different initial vibrational states at a given  $E_{\text{coll}}$ ; here the largest values are given for each  $E_{\text{coll}}$ .

<sup>c</sup>At  $E_{\text{coll}} = 50$  kcal/mol, 25 000 trajectories are run at each  $b$  in order to get improved statistics for the correlated differential cross sections and mode-specific product-state distributions.

negligible. Thus, we consider both the soft and hard ZPE constraints in which trajectories are discarded if the sum of the product vibrational energies is less than the sum of their ZPEs (soft) and either product has less vibrational energy than its ZPE (hard).

As mentioned above and shown in Table I, we run trajectories at equidistantly sampled  $b$  values, i.e.,  $b_n = n \times \Delta b$  [ $n = 0, 1, \dots, n_{\text{max}}$ ], where  $n_{\text{max}} = b_{\text{max}}/\Delta b$ . Therefore, cross sections are calculated by a  $b$ -weighted numerical integration of the reaction probabilities,  $P(b)$ , as

$$\sigma = \pi \sum_{n=1}^{n_{\text{max}}} \Delta b [b_n P(b_n) + b_{n-1} P(b_{n-1})]. \quad (1)$$

Differential cross sections as well as translational, vibrational, and rotational-vibrational distributions are also computed using Eq. (1) after binning the trajectories with respect to scattering angle, product relative translational energy, vibrational, and ro-vibrational state.

## B. Mode-specific normal mode analysis

Mode-specific vibrational analysis is performed for the  $N$ -atomic polyatomic products ( $\text{CHD}_2\text{F}$ ,  $\text{CD}_2\text{Cl}^-$ , and  $\text{CHDCl}^-$ ) following the procedure described in Ref. 21. The key steps of our approach can be summarized as follows:

- (1) A normal-mode analysis is carried out at the equilibrium geometry ( $\mathbf{r}_i^{\text{eq}}$ ), which provides  $3N - 6$  nonzero harmonic frequencies,  $\omega_k$  and the orthogonal transformation matrix, which transforms from Cartesian to normal coordinates.
- (2) We remove the angular momentum by modifying velocities.
- (3) For each trajectory, an exact transformation to the Eckart frame corresponding to  $\mathbf{r}_i^{\text{eq}}$  is done.
- (4) The normal coordinates ( $Q_k$ ) and momenta ( $P_k$ ) are determined from the mass-scaled Cartesian displacement coordinates and velocities using the transformation matrix obtained in step (1).

- (5) The harmonic vibrational energy and the corresponding action for each normal mode are obtained (in atomic units) as

$$E_k = \frac{P_k^2}{2} + \frac{\omega_k^2 Q_k^2}{2} \quad \text{and} \quad n'_k = \frac{E_k}{\omega_k} - \frac{1}{2} \quad (2)$$

$$k = 1, 2, \dots, 3N - 6.$$

The integer vibrational quanta ( $n_k$ ) are the nearest integer values of  $n'_k$ . Note that step (1) has to be done only once for a given product type, whereas steps (2)–(5) need to be repeated for each reactive trajectory.

## C. Binning techniques

The standard QCT studies apply the histogram binning (HB) technique, where the probability of a particular vibrational state  $\mathbf{n}$  at a given impact parameter is defined as

$$P_{\text{HB}}(b, \mathbf{n}) = \frac{N(b, \mathbf{n})}{N_{\text{traj}}(b)}, \quad (3)$$

where  $N(b, \mathbf{n})$  is the number of products in state  $\mathbf{n}$  from the total number of trajectories  $N_{\text{traj}}(b)$  at a specific  $b$  value.

Using the 1GB approach,<sup>20–22</sup> a Gaussian weight is defined for each product at a given  $b$  as

$$G_p(b, \mathbf{n}) = \frac{\beta}{\sqrt{\pi}} e^{-\beta^2 \left( \frac{E(\mathbf{n}'_{p,b}) - E(\mathbf{n})}{2E(\mathbf{0})} \right)^2} \quad p = 1, 2, \dots, N(b, \mathbf{n}), \quad (4)$$

where  $\beta = 2\sqrt{\ln 2}/\delta$ ,  $\delta$  is the full-width at half-maximum,  $E(\mathbf{n}'_{p,b})$  is the actual vibrational energy of the  $p^{\text{th}}$  product molecule,  $E(\mathbf{n})$  is the quantum energy corresponding to the vibrational state  $\mathbf{n}$  that is the nearest integer vector of  $\mathbf{n}'_{p,b}$ , and  $E(\mathbf{0})$  is the harmonic ZPE. Then, the probability of  $\mathbf{n}$  at a fixed  $b$  value can be obtained as

$$P_{\text{GB}}(b, \mathbf{n}) = \frac{\sum_{p=1}^{N(b, \mathbf{n})} G_p(b, \mathbf{n})}{N_{\text{traj}}(b)}. \quad (5)$$

Following Ref. 21, here we consider two 1GB approaches, denoted as GB(harm) and GB(harm-exact), to calculate  $G_p(b, \mathbf{n})$  by using different methods to calculate the energies  $E(\mathbf{n}'_{p,b})$  and  $E(\mathbf{n})$  used in Eq. (4).

GB(harm) employs the harmonic (harm) energy formulae for both  $E(\mathbf{n}'_{p,b})$  and  $E(\mathbf{n})$  as follows:

$$E(\mathbf{n}'_{p,b}) = \sum_{k=1}^{3N-6} \omega_k \left( n'_{k,p,b} + \frac{1}{2} \right) \quad (6)$$

and

$$E(\mathbf{n}) = \sum_{k=1}^{3N-6} \omega_k \left( n_k + \frac{1}{2} \right). \quad (7)$$

GB(harm-exact) determines  $E(\mathbf{n}'_{p,b})$  exactly in the Cartesian space as

$$E(\mathbf{n}'_{p,b}) = \frac{1}{2} \sum_{i=1}^N m_i \mathbf{v}_{i,p,b}^{\text{nr}} (\mathbf{v}_{i,p,b}^{\text{nr}})^T + V(\mathbf{r}_{1,p,b}, \mathbf{r}_{2,p,b}, \dots, \mathbf{r}_{N,p,b}) - V(\mathbf{r}_1^{\text{eq}}, \mathbf{r}_2^{\text{eq}}, \dots, \mathbf{r}_N^{\text{eq}}), \quad (8)$$

where  $v_{i,p,b}^{\text{tr}}$  is the velocity of the  $p$ th product at a given  $b$  and  $\mathbf{n}$  corresponding to zero angular momentum and  $V$  is the potential energy of the  $N$ -atomic product. This GB(harm-exact) approach uses the “exact” anharmonic Eq. (8) and the “harm” Eq. (7) for  $E(\mathbf{n}'_{p,b})$  and  $E(\mathbf{n})$ , respectively.

The vibrational mode specific cross sections are computed from  $P_{\text{HB}}(b, \mathbf{n})$  and  $P_{\text{GB}}(b, \mathbf{n})$  using a  $b$ -weighted integration utilizing Eq. (1). Note that we used the same approach in our previous studies, e.g., Refs. 20 and 21, even if the impact parameter treatment was not emphasized in the earlier work.

### III. RESULTS AND DISCUSSION

The  $\text{F}^- + \text{CHD}_2\text{Cl} \rightarrow \text{Cl}^- + \text{CHD}_2\text{F}$   $\text{S}_{\text{N}}2$  reaction is highly exothermic,  $\Delta H_0 = -10794 \text{ cm}^{-1}$  ( $-30.9 \text{ kcal/mol}$ ), whereas the proton abstraction channels leading to either  $\text{HF} + \text{CD}_2\text{Cl}^-$  or  $\text{DF} + \text{CHDCl}^-$  are endothermic with  $\Delta H_0 = 8709 \text{ cm}^{-1}$  ( $24.9 \text{ kcal/mol}$ ) or  $8778 \text{ cm}^{-1}$  ( $25.1 \text{ kcal/mol}$ ), as seen in Figure 2. Fig. 2 also shows the fundamental vibrational states of the reactant and the various product molecules and ions. In this study, we focus on the ground, CH-, and CD-stretch excited ( $v_{\text{CH}}(a') = 1$ ,  $v_{\text{CD}}(a') = 1$ , and  $v_{\text{CD}}(a'') = 1$ ) vibrational states of the reactant and we investigate the mode-specific overall as well as state-to-state reactivity. Before we move forward, we examine how the reactant molecule maintains its initial mode-specific quasi-classical vibrational state while the reactants approach each other. Figure 3 shows the time evolution of the mode-specific vibrational energies of  $\text{CHD}_2\text{Cl}$  obtained by the procedure described in Sec. II B. As seen, most of the mode energies remain nearly

steady prior to collision, except the  $v_{\text{CD}}(a')$  stretching mode ( $2255 \text{ cm}^{-1}$ ) which loses energy and an  $a'$ -symmetry bending mode ( $1107 \text{ cm}^{-1}$ ) which gains energy. Due to the local-mode nature of the CH stretching, the  $\text{CHD}_2\text{Cl}(v_{\text{CH}}(a') = 1)$  reactant maintains its mode-specific excited character very well, only about 10% energy leakage is expected prior to reaction. In the case of the CD stretching-excited reactants, the energy leak is modest, about 20%, for  $v_{\text{CD}}(a'') = 1$  and more substantial, close to 50% during 0.3 ps, for  $v_{\text{CD}}(a') = 1$ ; nevertheless, the mode-specific excitations are still qualitatively described. Thus, Figure 3 shows that the QCT method can be used to study the mode-specific dynamics of  $\text{S}_{\text{N}}2$  and proton-abstraction reactions of methyl-halides.

#### A. $\text{S}_{\text{N}}2$ channel with inversion and retention

##### 1. Inversion cross sections

The mode-specific excitation functions (cross sections vs.  $E_{\text{coll}}$ ) of the halogen substitution channel are shown in Figure 4. As seen in our previous studies on the  $\text{F}^- + \text{CH}_3\text{Cl}$   $\text{S}_{\text{N}}2$  reaction,<sup>4,9</sup> the cross sections are very large at low collision energies and rapidly decrease with increasing  $E_{\text{coll}}$ . This is expected in the case of a highly exothermic barrierless (submerged barrier) reaction, where the attractive long range interactions play a key role at low  $E_{\text{coll}}$ . Cross section ratios between the stretching-excited and ground-state reactions are in the 0.9–1.3 range depending on  $E_{\text{coll}}$  as also shown in Fig. 4. At low  $E_{\text{coll}}$  (1–7 kcal/mol), the CH and CD stretching excitations slightly inhibit the  $\text{S}_{\text{N}}2$  reaction, at around 15 kcal/mol significant enhancement is seen, and at high  $E_{\text{coll}}$  the enhancement effect diminishes and turns

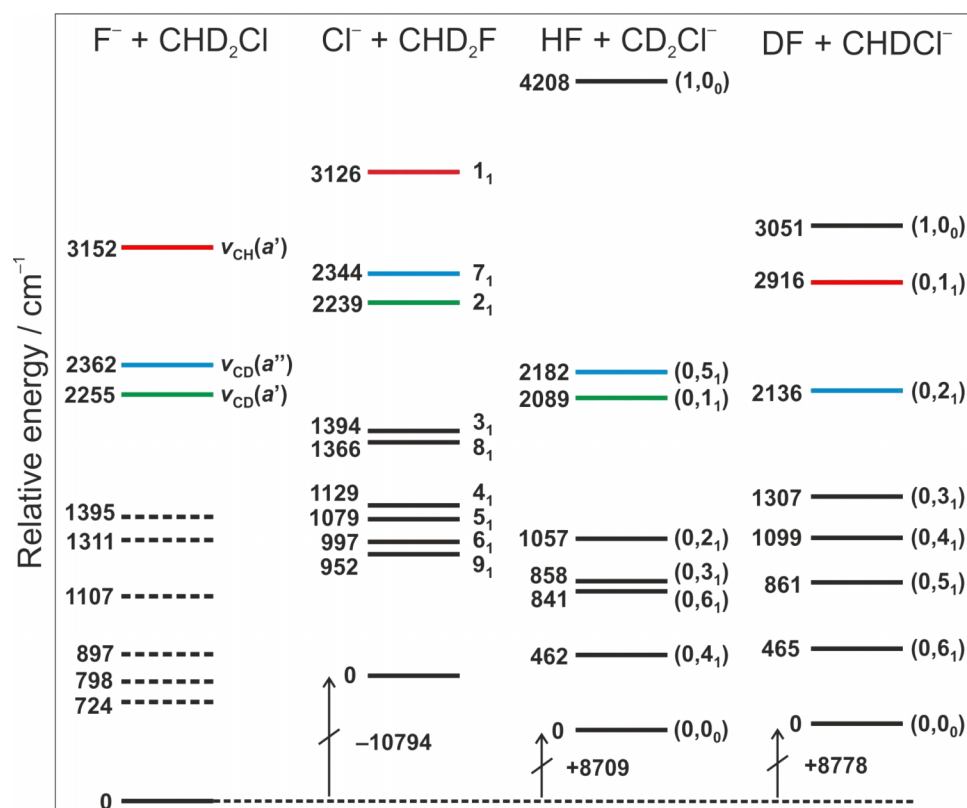


FIG. 2. Energetics of the  $\text{F}^- + \text{CHD}_2\text{Cl}$  reactions showing the initial and final fundamental harmonic vibrational states corresponding to the analytical PES (Ref. 4).

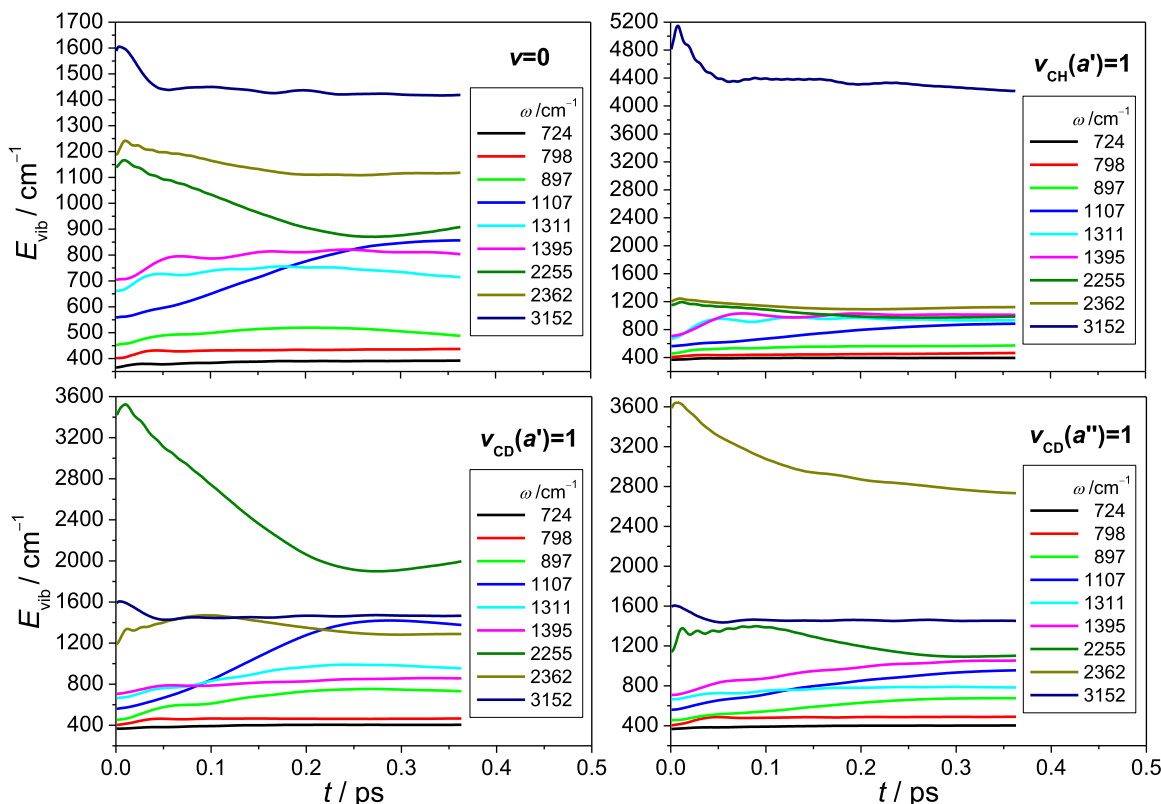


FIG. 3. Vibrational energies corresponding to the normal modes of ground-state ( $v=0$ ), CH stretching ( $v_{\text{CH}}(a')=1$ ), and CD stretching ( $v_{\text{CD}}(a')=1$  and  $v_{\text{CD}}(a'')=1$ ) excited  $\text{CHD}_2\text{Cl}$  as a function of the trajectory integration time. The vibrational energies are averaged over 500 trajectories and the time interval  $[0, t]$ . The  $\text{F}^-$  nucleophile is placed far, i.e., there is no interaction between the reactants. The harmonic vibrational frequencies of  $\text{CHD}_2\text{Cl}$  correspond to the analytical PES.

into inhibition. Despite the conventional wisdom saying that the CH stretching is a spectator mode in  $\text{S}_{\text{N}}2$  reactions, we find significant CH and CD stretching effects on the  $\text{S}_{\text{N}}2$  reactivity. Of course, QCT can overestimate these stretching effects due to unphysical energy leak from the excited mode to the other modes of the reactant molecule. This energy leak is likely the reason of the larger enhancement effect

found for the  $v_{\text{CD}}(a')=1$  excitation relative to  $v_{\text{CD}}(a'')=1$ . As discussed above, energy leak is the most substantial from the  $v_{\text{CD}}(a')=1$  mode, which may result in unphysical energy transfer to the reaction coordinate, thereby enhancing the  $\text{S}_{\text{N}}2$  reaction. Nevertheless, the present CH and CD stretching effects are certainly not just artifacts of the QCT method, because a recent quantum dynamical study<sup>19</sup> found similar CH stretching effect for the  $\text{F}^- + \text{CH}_3\text{Cl}$   $\text{S}_{\text{N}}2$  reaction.

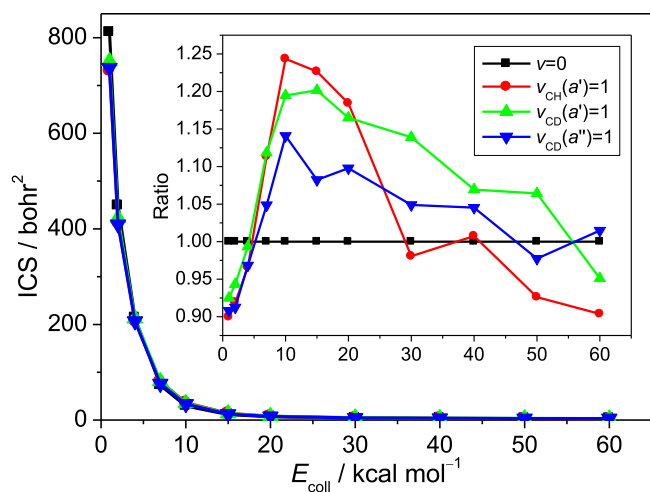


FIG. 4. Integral cross sections and their ratios,  $\text{ICS}/\text{ICS}(v=0)$ , as a function of collision energy for the ground-state, CH-stretching ( $v_{\text{CH}}(a')=1$ ), and CD-stretching ( $v_{\text{CD}}(a')=1$  and  $v_{\text{CD}}(a'')=1$ ) excited  $\text{F}^- + \text{CHD}_2\text{Cl} \rightarrow \text{CHD}_2\text{F} + \text{Cl}^-$  substitution reaction.

## 2. Retention cross sections

As mentioned in Sec. I, we recently discovered a double-inversion mechanism for the  $\text{F}^- + \text{CH}_3\text{Cl}$   $\text{S}_{\text{N}}2$  reaction, which is an indirect process involving several steps.<sup>4</sup> First,  $\text{F}^-$  abstracts a proton from  $\text{CH}_3\text{Cl}$  forming a  $\text{FH} \cdots \text{CH}_2\text{Cl}^-$  complex. Second,  $\text{HF}$  moves around the  $\text{CH}_2\text{Cl}^-$  unit and eventually the proton is transferred back forming a new CH bond while an umbrella motion inverts the configuration around the carbon center. Third, a second inversion occurs via the usual central transition state while the halogens exchange forming the  $\text{CH}_3\text{F} + \text{Cl}^-$  products with overall retention of configuration. Double-inversion cross sections as a function of  $E_{\text{coll}}$  are shown in Figure 5 for the ground-state and CH/CD stretching-excited  $\text{F}^- + \text{CHD}_2\text{Cl}$   $\text{S}_{\text{N}}2$  reactions. The double-inversion cross sections are about two orders of magnitude smaller than the inversion ones. For the  $\text{F}^- + \text{CHD}_2\text{Cl}(v=0)$  reaction, the double-inversion pathway opens at around  $E_{\text{coll}} = 15$  kcal/mol, in accord with its adiabatic barrier height of about 13 kcal/mol. The double-inversion excitation function

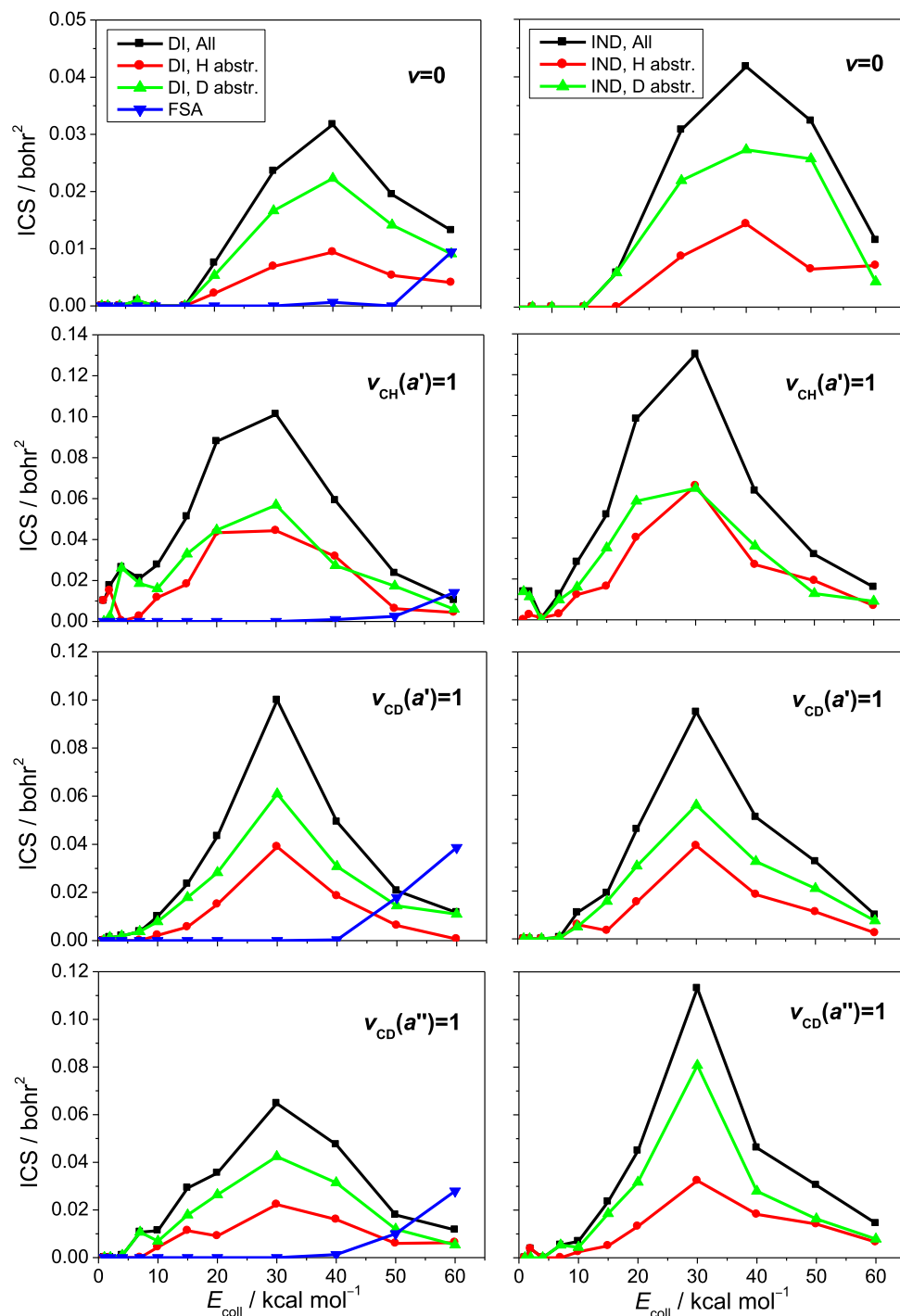


FIG. 5. Integral cross sections as a function of collision energy for the ground-state, CH-stretching ( $v_{\text{CH}}(a')=1$ ), and CD-stretching ( $v_{\text{CD}}(a')=1$  and  $v_{\text{CD}}(a'')=1$ ) excited retention mechanisms via double inversion (DI) and front-side attack (FSA) (left panels) and induced inversion (IND) of the  $\text{CHD}_2\text{Cl}$  reactant (right panels). For DI and IND, the H and D abstraction induced inversion pathways are identified.

increases with  $E_{\text{coll}}$ , has a maximum at 40 kcal/mol, and then decay is seen. The front-side attack retention pathway opens at  $E_{\text{coll}} = 50$  kcal/mol; thus, at low collision energies, the double-inversion mechanism is responsible for retention.

We have managed to distinguish between double inversions via H- or D-abstraction induced inversion. As shown in Figure 6, we followed the CH and CD distances in time for all the double-inversion trajectories and determined whether proton or deuteron abstraction induces the inversion of the  $\text{CD}_2\text{Cl}^-$  or  $\text{CHDCl}^-$  unit. The induced inversion is

verified by defining an angle between the C–Cl vector and the normal vector of the  $\text{CD}_2$  or  $\text{CHD}$  plane, as shown in Fig. 6. In order to provide additional insight into the double-inversion mechanism, Figure 6 also shows the distribution of the intermolecular CH/CD distances at the turning point of the inversion, where  $\text{CD}_2\text{Cl}^-/\text{CHDCl}^-$  is planar. As seen, the distribution is broad ranging from 1 to 5 Å and peaking at around 1.4 Å. Thus, in the most cases, the inversion occurs at shorter CH/CD distances than the corresponding double-inversion transition-state value of 1.8 Å.<sup>4</sup> Of course, this is

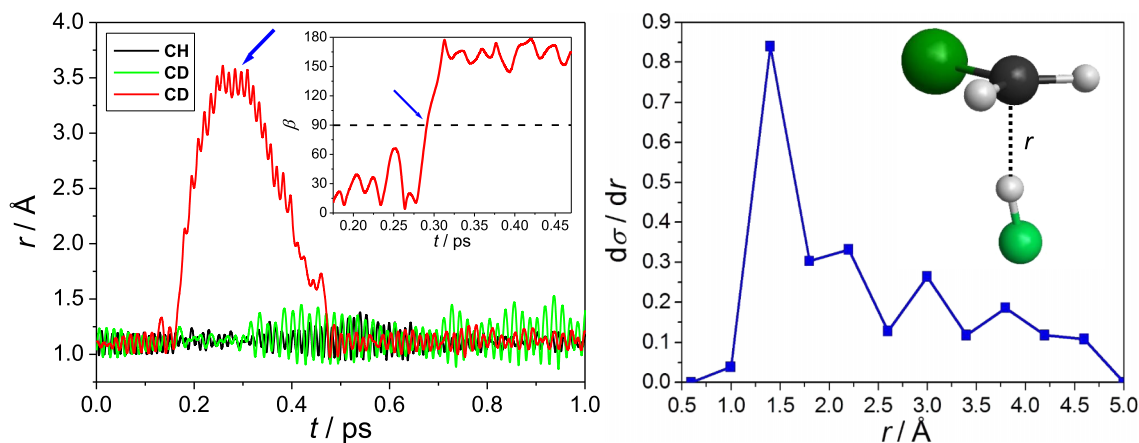


FIG. 6. CH and CD distances as a function of integration time for a double-inversion trajectory (left panel). The abstracted hydrogens (H or D) can be unambiguously distinguished based on the  $\beta$  angle defined as the angle between the C–Cl vector and the normal vector of the X–C–Y plane in the ClCXY moiety, where X = D and Y = H or D. The blue arrow indicates the representative case of D abstraction induced inversion, i.e., flipping of the H and D atoms in ClCHD via  $\beta = 90^\circ$ . Normalized distribution of the intermolecular CH/CD distances at  $\beta = 90^\circ$  for the  $F^- + \text{CHD}_2\text{Cl}(v = 0)$  reaction at collision energy of 50 kcal/mol (right panel).

somewhat expected, because the geometry at the saddle point is in slightly “pre-inversion” stage. Furthermore, it is important to find that significant number of induced inversions occur at large inter-fragment separations, where the proton/deuteron bonds back after the inversion of the  $\text{CD}_2\text{Cl}^-/\text{CHDCl}^-$  unit.

For the  $F^- + \text{CHD}_2\text{Cl}(v = 0)$  reaction, the ratio of the proton and deuteron abstraction induced double inversions is close to the statistical 1:2, as seen in Fig. 5. The CH and CD stretching excitations significantly enhance the double inversion. For  $F^- + \text{CHD}_2\text{Cl}(v_{\text{CH}} = 1)$ , the proton and deuteron abstraction pathways are not statistical, since the two pathways have similar cross sections, because CH stretching excitation has a larger enhancement effect on the proton abstraction induced mechanism. In the case of CD stretching excitations, an overall enhancement is seen, but the deuteron abstraction induced pathway is not getting additional preference. This may be due to the faster energy leak from the excited CD stretching modes relative to the CH mode. Furthermore, in the case of the CH stretching excitation, larger enhancement is expected, because the CH excitation energy is roughly 1.4 times larger than the CD energy. In Figure 5, we also show the cross sections for induced inversion that is not followed by halogen substitution, thereby resulting in an inverted  $\text{CHD}_2\text{Cl}$ . As seen, the induced-inversion cross sections have similar magnitudes and collision energy dependence as the double-inversion ones. This shows that there is roughly a fifty-fifty chance that the first inversion is followed by a substitution causing a second inversion.

## B. Proton and deuteron abstraction channels

### 1. Cross sections

Excitation functions for the proton and deuteron abstraction channels are given in Figure 7. The excitation functions of the HF and DF channels of the  $F^- + \text{CHD}_2\text{Cl}(v = 0)$  reaction increase from a threshold energy as  $E_{\text{coll}}$  increases and the cross sections of the two channels are virtually the same. This latter finding about the non-statistical HF:DF ratio shows that the probability of the proton transfer

is significantly higher than that of the deuteron abstraction. (Note that the same reactivity of H and D would result in a HF:DF ratio of 1:2.) CH stretching excitation substantially enhances the HF channel and with a lesser extent enhances the DF channel as well. For example, at  $E_{\text{coll}} = 40$  kcal/mol, the enhancement factors are 10 and 2 for the HF and DF channels, respectively. The CD stretching excitations also enhance the abstraction channels, but the effects are less significant than in the case of the CH excitation. At  $E_{\text{coll}} = 40$  kcal/mol, the enhancement factors are about 3–4 and 2–3 for the DF and HF channels, respectively. The soft and hard ZPE constraints decrease the absolute cross sections, but the shape of the excitation functions and the relative cross sections, i.e., vibrational enhancement factors, are virtually not affected, as shown in Figure 7. Thus, it is comforting that most of the qualitative conclusions do not depend on the ZPE treatment of the quasiclassical product analysis. However, one important advantage of the ZPE constraint should be mentioned. Without ZPE treatment, QCT underestimates the threshold energy due to ZPE violation of the products. For example, for the  $F^- + \text{CHD}_2\text{Cl}(v = 0)$  reaction, a few abstraction trajectories are found at  $E_{\text{coll}} = 20$  kcal/mol, even if the adiabatic(classical) barrier heights of the HF/DF channels are 24.9/25.1(28.2) kcal/mol corresponding to the analytical PES. The ZPE constraints, even in the soft case, increase the threshold energies and ensure physically realistic values.

### 2. Angular distributions and mechanisms

Scattering angle and initial attack angle distributions for the abstraction channels are shown in Figure 8. The scattering angle distributions are virtually the same for the HF and DF channels and show preference at backward direction (rebound mechanism) while the probability of sideways and forward scattering (stripping mechanism) is also significant. The attack angle, which is defined as the angle between the C–Cl vector and the initial velocity of  $\text{CHD}_2\text{Cl}$ , distributions show that the reaction can occur via front-side (Cl side) attack, but back-side ( $\text{CHD}_2$  side) collisions are preferred.

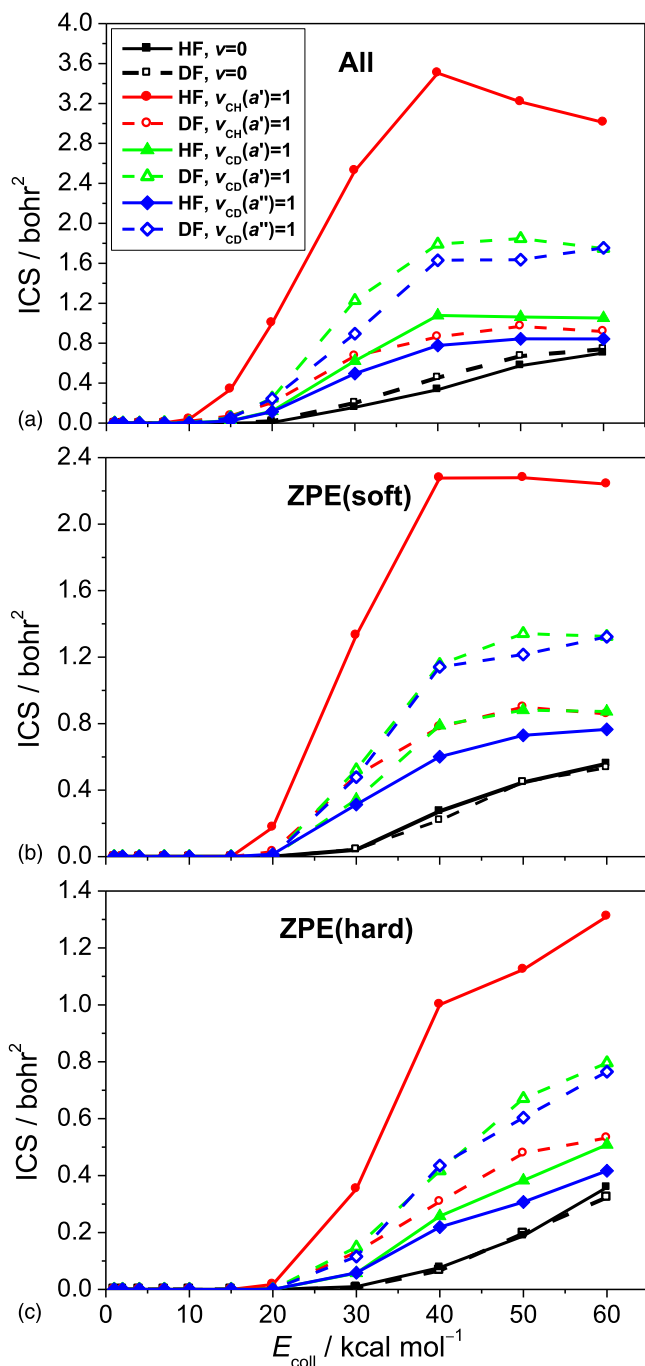


FIG. 7. Integral cross sections as a function of the collision energy for the ground-state ( $v=0$ ), CH-stretching ( $v_{\text{CH}}(a')=1$ ), and CD-stretching ( $v_{\text{CD}}(a')=1$  and  $v_{\text{CD}}(a'')=1$ ) excited  $\text{F}^- + \text{CHD}_2\text{Cl} \rightarrow \text{CD}_2\text{Cl}^- + \text{HF}$  and  $\text{F}^- + \text{CHD}_2\text{Cl} \rightarrow \text{CHDCl}^- + \text{DF}$  abstraction reactions, considering (a) all trajectories (All) without ZPE constraint, (b) ZPE(soft) constraint where trajectories are discarded if the sum of the product vibrational energies is less than the sum of their ZPEs, and (c) ZPE(hard) constraint where trajectories are discarded if either product has less vibrational energy than its ZPE.

Unlike for the scattering angles, in the case of the attack angle distributions, a significant difference is seen between the HF and DF channels. For the DF channel, the back-side and front-side attacks, i.e., end-on collisions, are more preferred, whereas the side-on collisions are less favored, compared to the HF channel. In order to get deeper insight into the mechanisms of the abstraction process, in Fig. 8 we

show the correlation diagrams of the scattering angle and attack angle distributions. These correlation diagrams reveal three major direct abstraction mechanisms, namely, back-side rebound, back-side stripping, and front-side stripping as the representative trajectory snapshots shown in Figure 9. Furthermore, the angle correlations show that the front-side rebound is not preferred. For the HF channel, the side-on rebound is also significant, whereas this mechanism is found to be negligible for the DF channel. Recently, without distinguishing between back-side and front-side attacks, Zhang, Xie, and Hase also identified rebound and stripping as the direct mechanisms of the proton transfer in  $\text{F}^- + \text{CH}_3\text{I}$ .<sup>24</sup>

### C. Energy transfer

It is an important question as how the initial translational and vibrational energies of the reactive system transfer to the translational, vibrational, and rotational degrees of freedom of the products. Answering this question is especially challenging for polyatomic products where many vibrational modes exist. Our mode-specific product analysis and advanced binning methods described in Secs. II B and II C provide insight into the mode-specific state-to-state dynamics of the title reaction. We focus below the proton and deuteron abstraction channels, but mode-specific product distributions are also presented for the  $\text{S}_{\text{N}}2$  channel. Besides following the energy transfer, we aim to test various binning methods (HB and different 1GB approaches), thereby showing their utilities and limitations.

#### 1. Translational energy distributions

Relative translational energy distributions for the HF +  $\text{CD}_2\text{Cl}^-$  and DF +  $\text{CHDCl}^-$  products of the ground-state and CH/CD stretching-excited  $\text{F}^- + \text{CHD}_2\text{Cl} \rightarrow \text{CD}_2\text{Cl}^- + \text{HF}$  and  $\text{F}^- + \text{CHD}_2\text{Cl} \rightarrow \text{CHDCl}^- + \text{DF}$  reactions at  $E_{\text{coll}} = 50$  kcal/mol ( $17\,500$   $\text{cm}^{-1}$ ) are shown in Figure 10. For the  $\text{F}^- + \text{CHD}_2\text{Cl}(v=0)$  reaction, the distributions are almost the same for the HF and DF channels, have a maximum at a low energy ( $1500$   $\text{cm}^{-1}$ ), and decrease sharply as the translational energy increases. In the case of the CH stretching-excited reactant, the HF distribution becomes much broader and hotter (almost constant up to  $10\,000$   $\text{cm}^{-1}$ ), whereas the DF channel is only slightly affected. Thus, it seems that most of the CH stretching excitation energy goes into translation of the products if the excited bond breaks. In the case of the CD stretching excitations, the distributions become slightly broader and hotter than the corresponding ones of the  $v=0$  reaction, but interestingly the distributions of the HF and DF channels are very similar, especially in the  $v_{\text{CD}}(a')=1$  case. This may partially be due to the facts that the CD stretching excitation energies are smaller than the CH energy and the energy leak is faster for the CD modes. Of course, the product vibrational distributions can shed more light on this interesting energy transfer as discussed below.

#### 2. Mode-specific polyatomic product vibrational distributions

Figure 11 shows the mode-specific vibrational distributions for the  $\text{CHD}_2\text{F}$  product of the  $\text{F}^- + \text{CHD}_2\text{Cl}(v_{\text{CH}}=0, 1)$   $\text{S}_{\text{N}}2$  reactions using the HB, GB(harm), and GB(harm-exact)

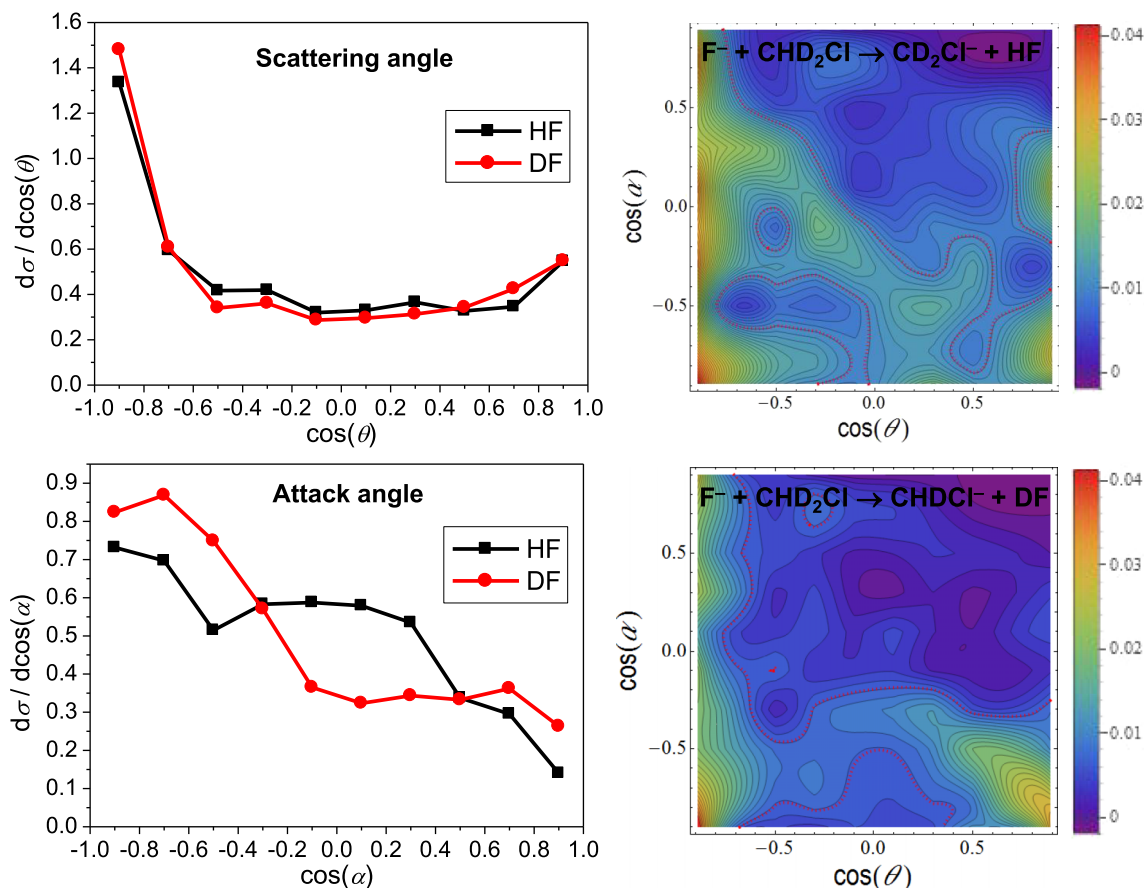


FIG. 8. Scattering angle and initial attack angle distributions (left panels) and their correlations (right panels) at collision energy of 50 kcal/mol for the  $F^- + \text{CHD}_2\text{Cl}(v=0) \rightarrow \text{CD}_2\text{Cl}^- + \text{HF}$  and  $F^- + \text{CHD}_2\text{Cl}(v=0) \rightarrow \text{CHDCl}^- + \text{DF}$  abstraction reactions considering all trajectories without ZPE constraint. The scattering angle ( $\theta$ ) is defined as the angle between the initial  $\text{CHD}_2\text{Cl}$  and the final HF or DF velocity vectors. The initial attack angle ( $\alpha$ ) is defined as the angle between the C–Cl vector and the velocity vector of  $\text{CHD}_2\text{Cl}$  at  $t=0$ .

binning techniques (see Sec. II C). Using HB we get small populations for vibrational states above the maximum available energy ( $E_{\text{max}}$ ) due to the rounding issue of the HB method and the occasional failure of the normal-mode analysis. In the former case, the possible rounding of the non-integer action to an upper integer quantum number can result in an energetically non-available state. The other issue is that the normal-mode analysis can overestimate the mode-specific

vibrational energy, especially at highly distorted structures, which can result in again an unphysical vibrational state. The GB(harm) method solves the rounding issue, but does not treat the normal-mode analysis issue. As Fig. 11 shows, GB(harm) slightly decreases the density of states above  $E_{\text{max}}$ , but the unphysical populations are still not negligible. If we use GB(harm-exact), which solves both issues, the undesired states above  $E_{\text{max}}$  disappear, as seen in Fig. 11. Besides the

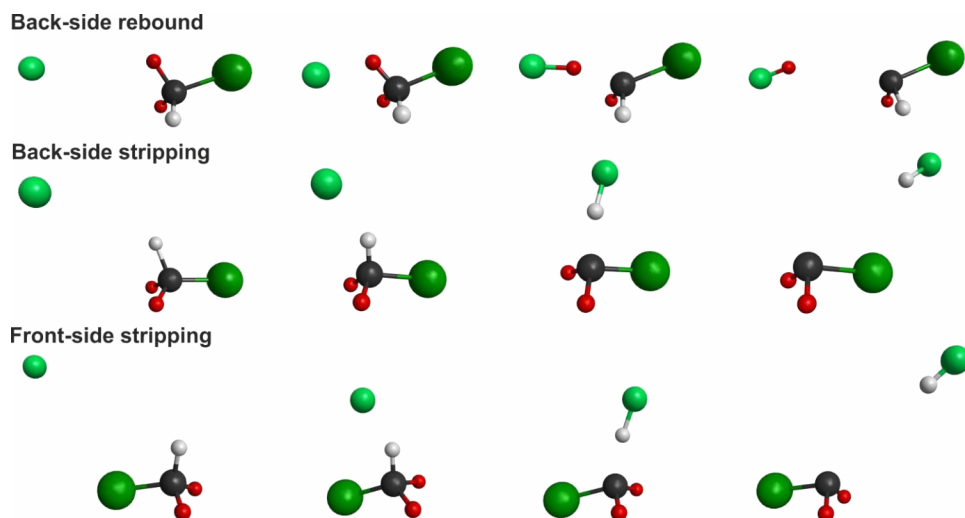


FIG. 9. Snapshots of representative abstraction trajectories at collision energy of 50 kcal/mol. Note that the front-side rebound mechanism is not favored as indicated by the correlated distribution of the scattering and initial attack angles in Figure 8.

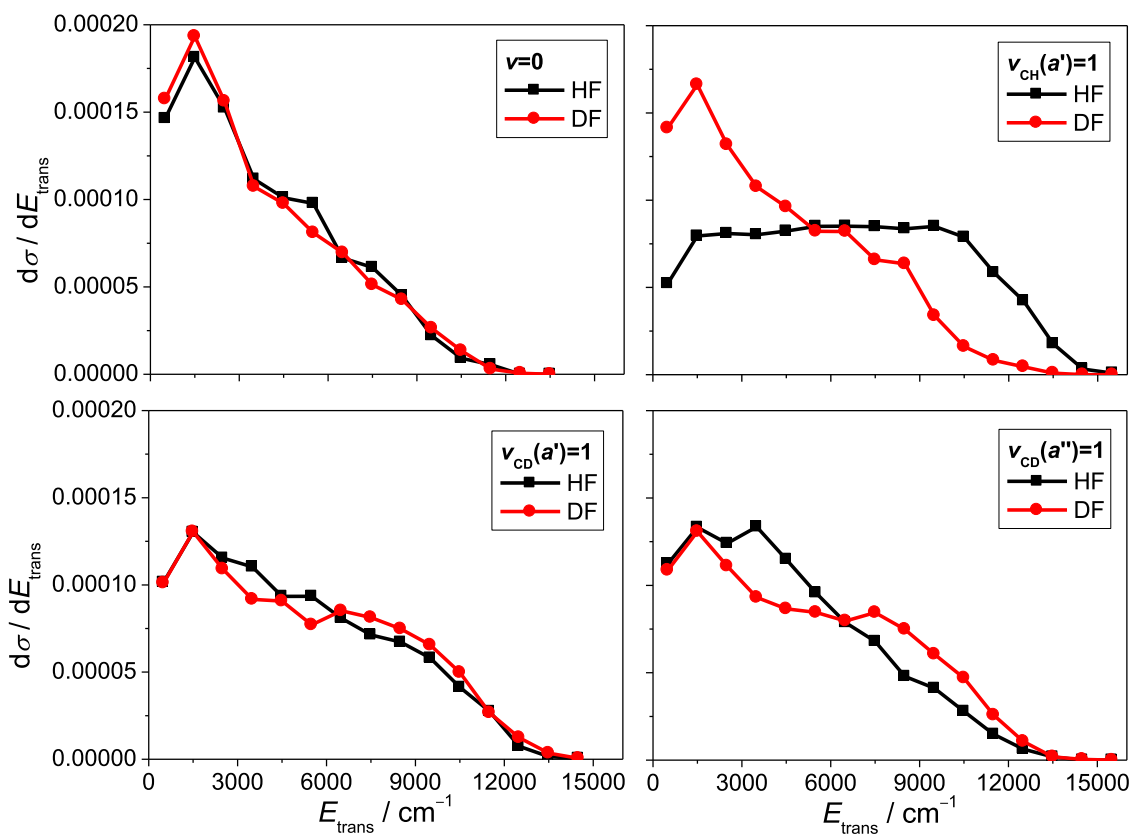


FIG. 10. Normalized product relative translational energy distributions at collision energy of 50 kcal/mol for the ground-state ( $v=0$ ), CH-stretching ( $v_{\text{CH}}(a')=1$ ), and CD-stretching ( $v_{\text{CD}}(a')=1$  and  $v_{\text{CD}}(a'')=1$ ) excited  $\text{F}^- + \text{CHD}_2\text{Cl} \rightarrow \text{CD}_2\text{Cl}^- + \text{HF}$  and  $\text{F}^- + \text{CHD}_2\text{Cl} \rightarrow \text{CHDCl}^- + \text{DF}$  abstraction reactions considering all trajectories without ZPE constraint.

above-discussed differences, all the binning techniques show that the ground vibrational state of  $\text{CHD}_2\text{F}$  has the highest probability for the  $\text{F}^- + \text{CHD}_2\text{Cl}(v=0)$  reaction, whereas  $\text{CHD}_2\text{F}(v=0)$  is negligible for  $\text{F}^- + \text{CHD}_2\text{Cl}(v_{\text{CH}}=1)$ , where the fundamental vibrational state with one quantum excitation on the CH stretching mode is the most likely one.

As GB(harm-exact) is found to be the most realistic, we use this approach to present the mode-specific vibrational distributions for the  $\text{CD}_2\text{Cl}^-$  and  $\text{CHDCl}^-$  products of the ground-state and CH/CD stretching-excited  $\text{F}^- + \text{CHD}_2\text{Cl}$  reactions in Figures 12 and 13. The weights for the diatom + polyatom channels are computed as the products of the 1GB weights of the fragments. The Gaussian weights for HF and DF are obtained based on their internal energy as described in Ref. 20. In all cases, even for the CH/CD stretching-excited reactions, the dominant product state is the ground vibrational state of  $\text{CD}_2\text{Cl}^-/\text{CHDCl}^-$ . Furthermore, some umbrella and bending excited states, including their overtones and combinations, have significant populations as indicated in Figs. 12 and 13. Interestingly, the  $\text{CD}_2\text{Cl}^-$  product is found vibrationally colder for the  $v_{\text{CH}}=1$  reaction than for the  $v=0$  reaction. Since, as discussed earlier,  $v_{\text{CH}}=1$  excitation makes the translational energy distribution of the  $\text{HF} + \text{CD}_2\text{Cl}^-$  channel much broader and hotter than that of the  $v=0$  reaction, it seems that the CH stretching-excitation energy preferably transfers into relative translation than

vibration of the products. (Note that possible energy transfer to HF ro-vibration will be discussed later.) In the case of the  $\text{DF} + \text{CHDCl}^-$  channel, the  $\text{F}^- + \text{CHD}_2\text{Cl}(v_{\text{CH}}=1)$  reaction produces vibrationally much hotter  $\text{CHDCl}^-$  products than the  $v=0$  reaction does. In the  $v_{\text{CH}}=1$  reaction, the CH stretching-excited state of  $\text{CHDCl}^-$  becomes the second most favored product state after ground state. However, it is important to note that the population of this state is not very large; thus, QCT shows that the CH stretching is not a pure spectator mode in the  $\text{F}^- + \text{CHD}_2\text{Cl}(v_{\text{CH}}=1) \rightarrow \text{DF} + \text{CHDCl}^-$  reaction. The breakdown of the spectator mode picture is even more obvious for the CD stretching-excited reactions, where the populations of the CD stretching-excited  $\text{CD}_2\text{Cl}^-$  product states are small. Unlike for  $\text{F}^- + \text{CHD}_2\text{Cl}(v_{\text{CH}}=1)$ , for the  $v_{\text{CD}}=1$  reactions, both the  $\text{CD}_2\text{Cl}^-$  and  $\text{CHDCl}^-$  vibrational distributions are somewhat hotter than the corresponding  $v=0$  distributions, in accord with the different CH and CD stretching effects on the translational energy distributions.

In order to get more insight into the mode-specific product state distributions, in Figure 14, we show the distributions of the vibrational quantum numbers on each specific mode of the  $\text{CHD}_2\text{F}$ ,  $\text{CD}_2\text{Cl}^-$ , and  $\text{CHDCl}^-$  products integrating over all the other modes. In the case of each product vibrational mode of the  $\text{F}^- + \text{CHD}_2\text{Cl}(v=0)$  reaction, the zero quantum is the most likely with about 50% probability for the lowest-energy mode(s) and about 90% probability for the highest-energy one(s). One-quantum excitation has

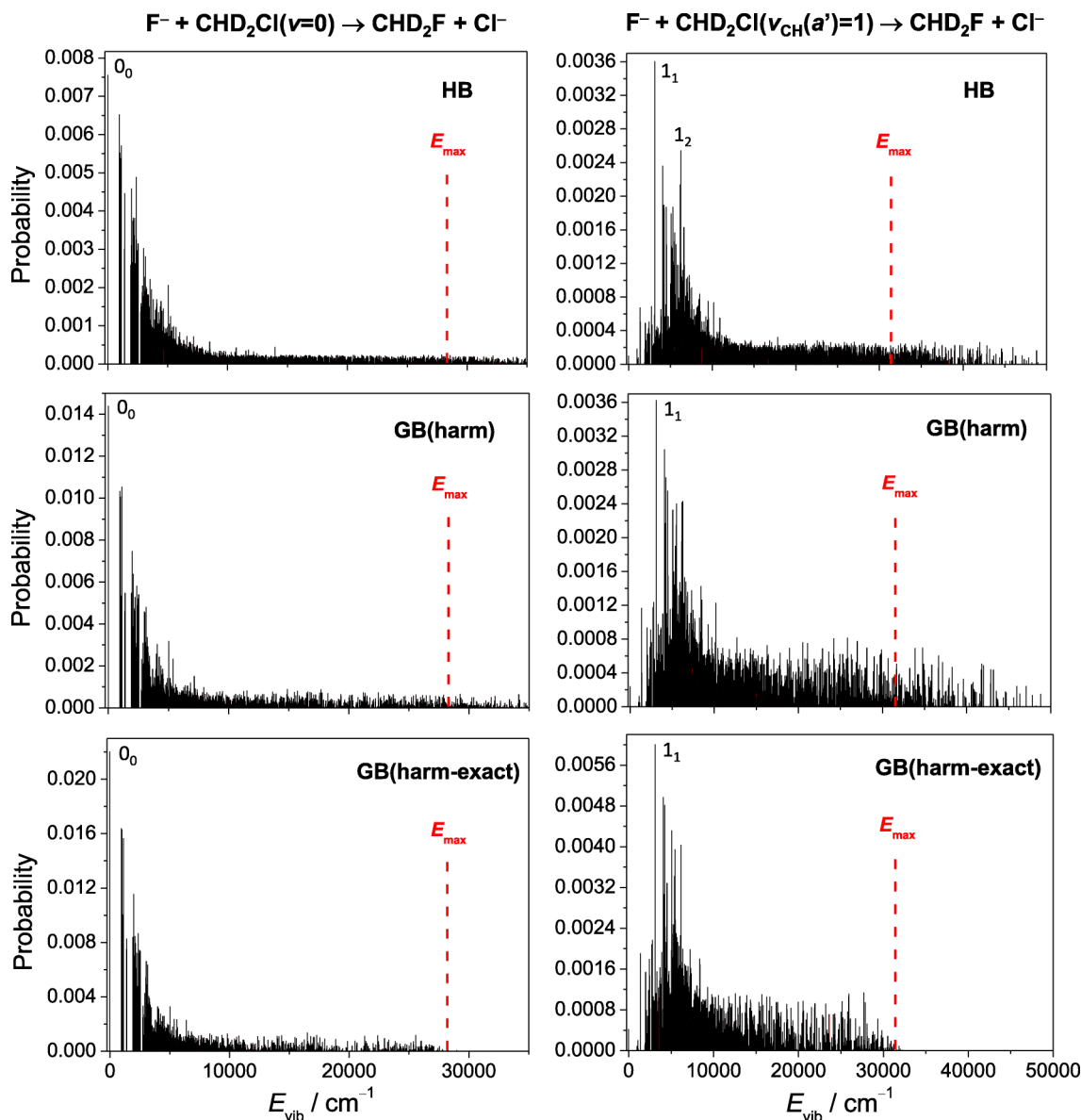


FIG. 11. Normalized  $\text{CHD}_2\text{F}$  mode-specific vibrational distributions (showing all the states) at collision energy of 50 kcal/mol for the ground-state ( $v=0$ ) and CH stretching-excited ( $v_{\text{CH}}(a')=1$ )  $\text{F}^- + \text{CHD}_2\text{Cl} \rightarrow \text{CHD}_2\text{F} + \text{Cl}^-$  substitution reactions. The vibrational energies are relative to the ZPE and the results are obtained by standard histogram binning (HB) and two versions of Gaussian binning (1GB), GB(harm) and GB(harm-exact), as described in Sec. II C. The red dashed lines indicate the maximum available energy ( $E_{\text{max}}$ ).  $0_0$ ,  $1_1$ , and  $1_2$  denote the ground, fundamental CH stretching, and first-overtone CH stretching states, respectively.

about 20%–30% probability for the low-energy bending and C–Cl stretching modes and usually less than 10% for the CH/CD stretching modes. Small populations for excitations with multiple quanta are also seen, especially for the low-energy modes. Figure 14 also shows the quantum number distributions for the  $\text{F}^- + \text{CHD}_2\text{Cl}(v_{\text{CH}}=1)$  reaction. The distributions are similar as described above for the  $v=0$  reaction, but important subtle differences can be observed. For the  $\text{CHD}_2\text{F}$  product of the  $\text{S}_{\text{N}}2$  channel, the probability of one-quantum excitation of the CH stretching mode increases from 6% to 32% and the ground state of the CH stretching drops from 93% to 65% upon  $v_{\text{CH}}=1$  excitation of the reactant. This finding shows that in some cases, the CH stretching excitation energy of reactant is conserved in the product, but the CH stretching is not always a spectator mode in the  $\text{S}_{\text{N}}2$  reaction. In the case of the proton-abstraction

channel, the vibrational quantum number distributions do not change significantly if we excite the CH stretching of the reactant, supporting our previous finding (Fig. 10) that the CH stretching excitation energy mainly transfers into product translation. For the deuteron-abstraction channel, the probability of one-quantum excitation on the CH stretching mode of  $\text{CHDCI}^-$  increases from 6% to 22% upon  $v_{\text{CH}}=1$  excitation of the reactant, but this mode is still not a pure spectator as we already concluded based on Fig. 13.

### 3. HF and DF rotational-vibrational distributions

Correlated HF and DF rotational-vibrational distributions for the ground-state and CH/CD stretching-excited  $\text{F}^- + \text{CHD}_2\text{Cl}$  reactions are shown in Figure 15. In all cases, even for the  $v_{\text{CH}}=1$  and  $v_{\text{CD}}=1$  reactions, the HF and

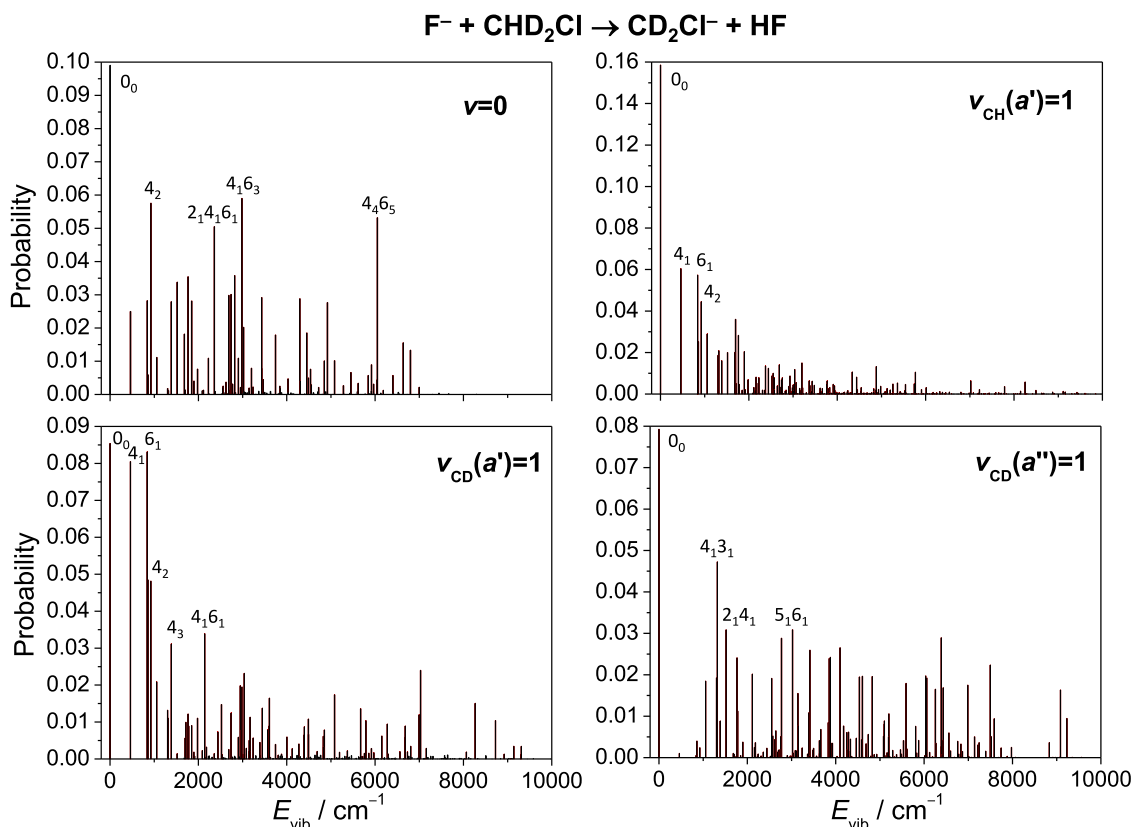


FIG. 12. Normalized  $CD_2Cl^-$  mode-specific vibrational distributions (showing all the states) at collision energy of 50 kcal/mol for the ground-state ( $v=0$ ), CH-stretching ( $v_{CH}(a')=1$ ), and CD-stretching ( $v_{CD}(a')=1$  and  $v_{CD}(a'')=1$ ) excited  $F^- + CHD_2Cl \rightarrow CD_2Cl^- + HF$  abstraction reactions. The vibrational energies are relative to the ZPE and the results are obtained by GB(harm-exact). See Figure 2 for the notation of the product states.

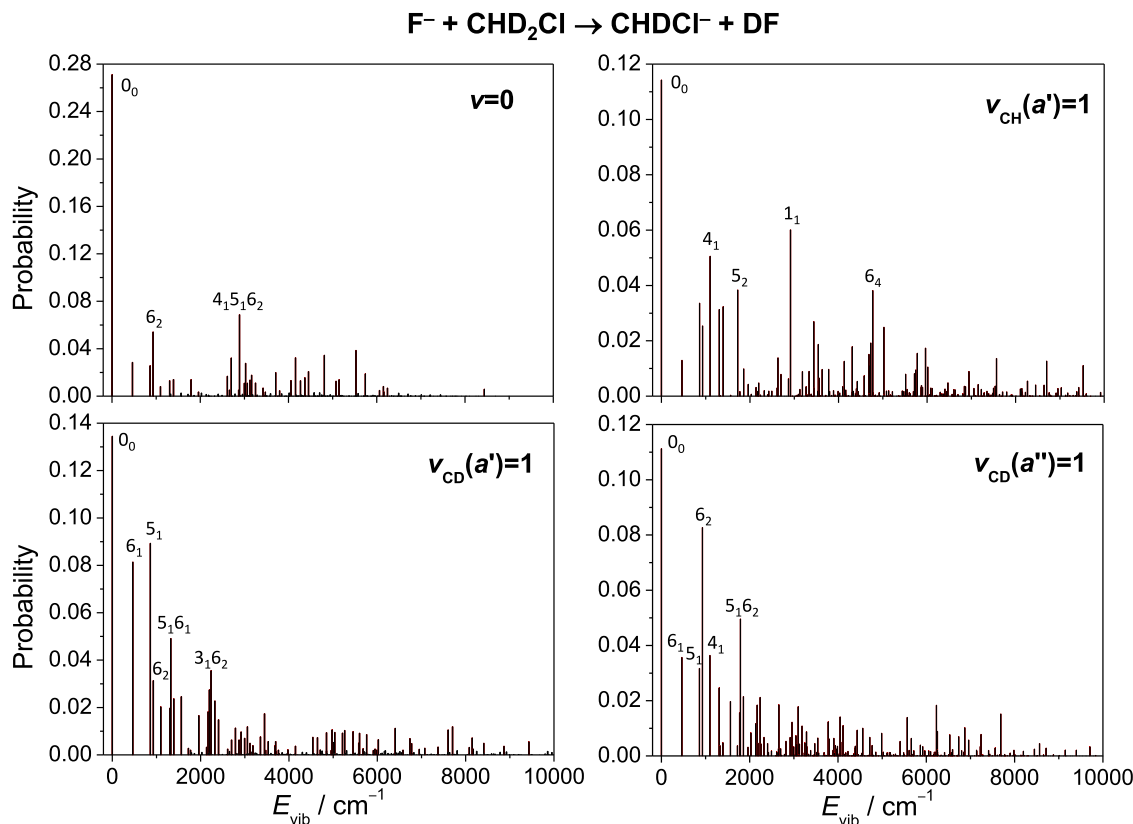


FIG. 13. Normalized  $CHDCl^-$  mode-specific vibrational distributions (showing all the states) at collision energy of 50 kcal/mol for the ground-state ( $v=0$ ), CH-stretching ( $v_{CH}(a')=1$ ), and CD-stretching ( $v_{CD}(a')=1$  and  $v_{CD}(a'')=1$ ) excited  $F^- + CHD_2Cl \rightarrow CHDCl^- + DF$  abstraction reactions. The vibrational energies are relative to the ZPE and the results are obtained by GB(harm-exact). See Figure 2 for the notation of the product states.

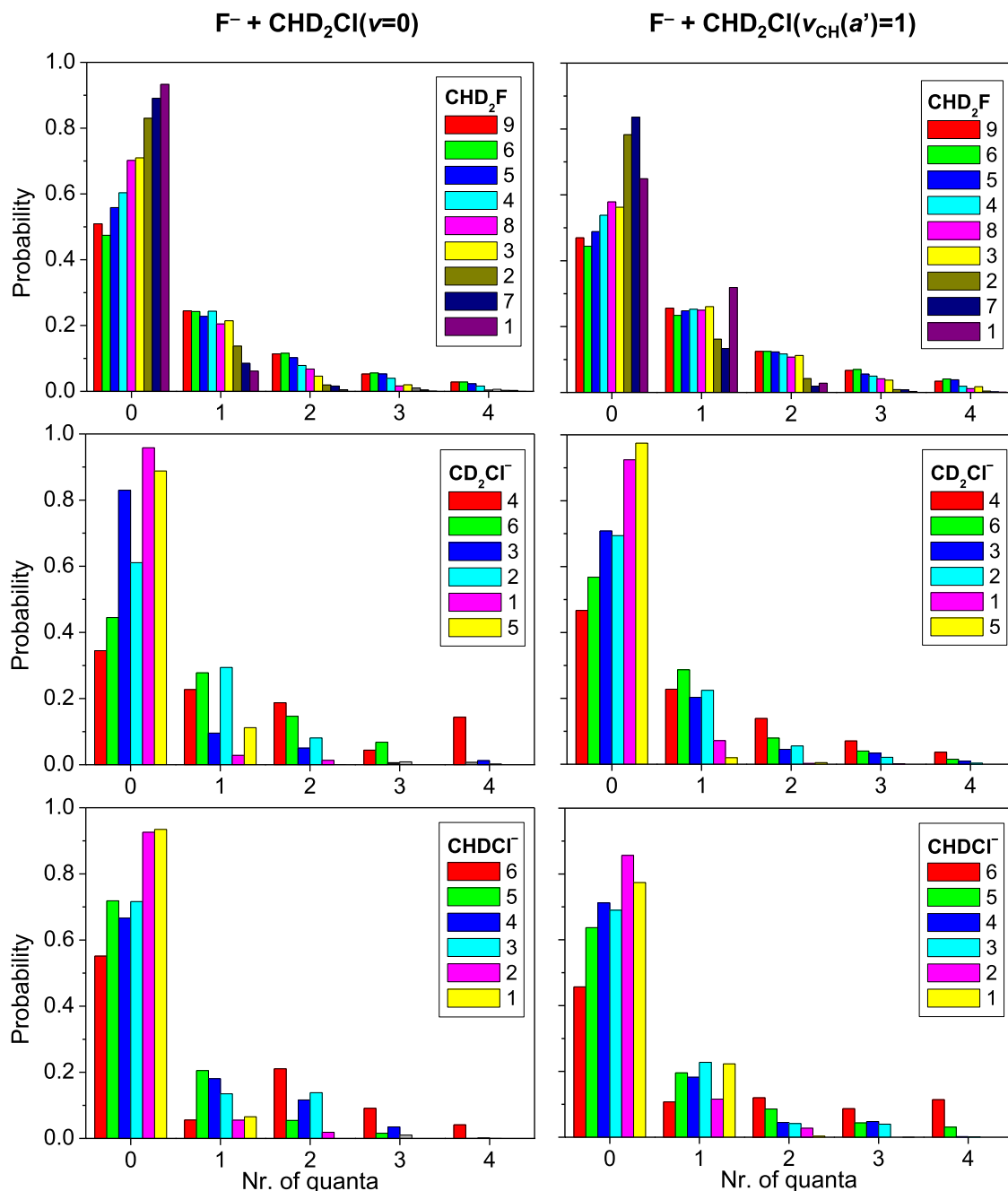


FIG. 14. Normalized distributions of the vibrational quantum states at collision energy of 50 kcal/mol for the CHD<sub>2</sub>F, CD<sub>2</sub>Cl<sup>-</sup> and CHDCI<sup>-</sup> products of the ground-state ( $v=0$ ) and CH stretching-excited ( $v_{\text{CH}}(a')=1$ ) F<sup>-</sup>+CHD<sub>2</sub>Cl reactions. The results are obtained by GB(harm-exact) and the vibrational quantum states are defined in Figure 2.

DF product molecules are rotationally and vibrationally cold favoring the ground vibrational state. At  $E_{\text{coll}} = 50$  kcal/mol, the populations of HF( $v=0$ ), HF( $v=1$ ), and HF( $v=2$ ) are about 83%, 15%, and 2%, respectively, with small variations depending on the initial state of the reactant. The DF products are slightly more excited, the fractions of DF( $v=0$ ), DF( $v=1$ ), and DF( $v=2$ ) are about 75%, 19%, and 4%, respectively, again with little initial-state dependence. For the HF channel, the rotational distributions peak at  $J=1$  and the most populated rotational states are  $J=0-3$  having a total of about 80% probability without any significant initial and/or final vibrational state dependence. This cold HF rotational distribution agrees almost

quantitatively with the HF( $J$ ) population of the F<sup>-</sup> + CH<sub>3</sub>I reaction at  $E_{\text{coll}} = 35$  kcal/mol.<sup>24</sup> In the case of the DF products of the F<sup>-</sup> + CHD<sub>2</sub>Cl reaction, the distributions slightly shift toward larger  $J$  values, as expected based on the smaller rotational constant of DF relative to that of the HF molecule. For DF, the  $J=1-4$  states have the highest populations (~65% altogether) peaking at  $J=2$ . Similar to the HF case, the DF rotational distributions do not show significant initial-state dependence and/or correlation to the product vibrational state. On the basis of the above findings, we can conclude that the initial vibrational and relative translational energy does not transfer significantly to the HF/DF vibration and rotation.

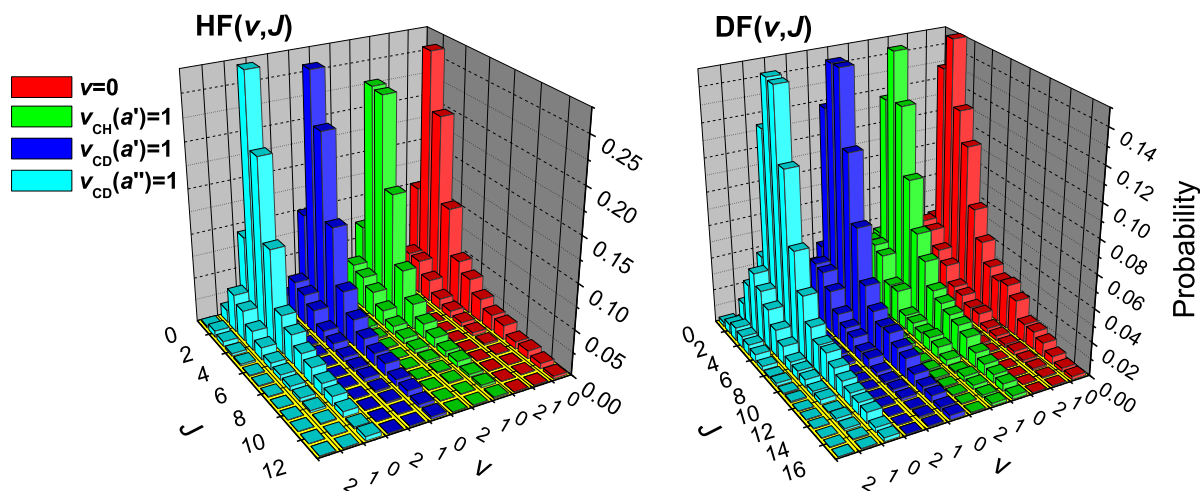


FIG. 15. Normalized rotational-vibrational distributions for HF( $v, J$ ) and DF( $v, J$ ) at collision energy of 50 kcal/mol for the ground-state ( $v = 0$ ), CH-stretching ( $v_{\text{CH}}(a') = 1$ ), and CD-stretching ( $v_{\text{CD}}(a') = 1$  and  $v_{\text{CD}}(a'') = 1$ ) excited  $\text{F}^- + \text{CHD}_2\text{Cl} \rightarrow \text{CD}_2\text{Cl}^- + \text{HF}$  and  $\text{F}^- + \text{CHD}_2\text{Cl} \rightarrow \text{CHDCI}^- + \text{DF}$  abstraction reactions considering all trajectories without ZPE constraint.

#### IV. SUMMARY AND CONCLUSIONS

We have studied the mode-specific dynamics of the ground-state and CH/CD stretching-excited  $\text{F}^- + \text{CHD}_2\text{Cl}$  reactions focusing on the  $\text{S}_{\text{N}}2$ , proton-, and deuteron-abstraction channels leading to  $\text{Cl}^- + \text{CHD}_2\text{F}$ ,  $\text{HF} + \text{CD}_2\text{Cl}^-$ , and  $\text{DF} + \text{CHDCI}^-$ , respectively. The efficient computation of more than  $6 \times 10^6$  trajectories has been made possible by using our recently developed full-dimensional *ab initio* global analytical PES.<sup>4</sup> The extremely large number of trajectories allows computing correlated differential cross sections and mode-specific product state and rotational-vibrational distributions with reasonable statistical accuracy. These new detailed QCT results provide deep insights into the multi-channel dynamics and various mechanisms of the title reaction as well as the energy transfer in the reactive system. The main conclusions of the present study can be summarized as follows:

- The CH stretching excitation energy of the reactant  $\text{CHD}_2\text{Cl}$  is well maintained prior to collision; whereas the energy leak from the CD stretching modes is more significant. Nevertheless, QCT can be used to study the mode-specific dynamics of the  $\text{F}^- + \text{CHD}_2\text{Cl}$  reaction.
- For the  $\text{S}_{\text{N}}2$  channel, slight vibrational inhibition is found at low and high collision energies, whereas enhancement is seen around the middle of the 1–60 kcal/mol collision energy range.
- Double-inversion pathways are found for the title reaction and substantially enhanced upon CH/CD stretching excitations. Double inversion via proton and deuteron abstraction occurs with almost statistical probability for the  $v = 0$  reaction, whereas initial CH stretching excitation favors the proton-abstraction induced pathway.
- The abstraction reactions produce HF and DF products with non-statistical ratio favoring the HF channel. CH and CD stretching excitations significantly enhance the corresponding abstraction channels, especially in the CH case. These findings are qualitatively the same with and without ZPE constraint.

- Correlated scattering and attack angle distributions reveal back-side rebound, back-side stripping, and front-side stripping mechanisms for the abstraction channels.
- 1GB approach based on exactly computed classical vibrational energies is shown to solve both the rounding and normal-mode analysis issues, therefore advocated for mode-specific polyatomic product analysis.
- For the abstraction channels, most of the initial translational and vibrational energy transfers into translation of the products, since the ground vibrational states of both the diatomic and polyatomic products have the highest probability. Neither CH nor CD stretching is found to be a pure spectator mode.
- The HF and DF products are rotationally cold favoring the  $J = 0-3$  and  $J = 1-4$  states, respectively, without any significant initial and/or final vibrational state specificity.

We hope that the present detailed QCT study will guide and motivate future experimental and quantum dynamical investigations of mode specificity and isotope effects in  $\text{S}_{\text{N}}2$  and proton/deuteron abstraction reactions.

#### ACKNOWLEDGMENTS

G.C. thanks the Scientific Research Fund of Hungary (Grant No. PD-111900) and the János Bolyai Research Scholarship of the Hungarian Academy of Sciences for financial support. We acknowledge the National Information Infrastructure Development Institute for awarding us access to the supercomputer based in Szeged, Hungary.

- P. Walden, *Ber. Dtsch. Chem. Ges.* **29**, 133 (1896).
- C. K. Ingold, *Structure and Mechanisms in Organic Chemistry* (Cornell University Press, Ithaca, NY, 1953).
- J. Xie, R. Otto, J. Mikosch, J. Zhang, R. Wester, and W. L. Hase, *Acc. Chem. Res.* **47**, 2960 (2014).
- I. Szabó and G. Czakó, *Nat. Commun.* **6**, 5972 (2015).
- M. Stei, E. Carrascosa, M. A. Kainz, A. H. Kelkar, J. Meyer, I. Szabó, G. Czakó, and R. Wester, *Nat. Chem.* **8**, 151 (2016).
- J. I. Brauman, *Science* **319**, 168 (2008).
- J. Xie and W. L. Hase, *Science* **352**, 32 (2016).

- <sup>8</sup>J. Mikosch, J. Zhang, S. Trippel, C. Eichhorn, R. Otto, R. Sun, W. A. de Jong, M. Weidemüller, W. L. Hase, and R. Wester, *J. Am. Chem. Soc.* **135**, 4250 (2013).
- <sup>9</sup>I. Szabó, A. G. Császár, and G. Czakó, *Chem. Sci.* **4**, 4362 (2013).
- <sup>10</sup>J. Mikosch, S. Trippel, C. Eichhorn, R. Otto, U. Lourderaj, J.-X. Zhang, W. L. Hase, M. Weidemüller, and R. Wester, *Science* **319**, 183 (2008).
- <sup>11</sup>M. N. Glukhovtsev, A. Pross, H. B. Schlegel, R. D. Bach, and L. Radom, *J. Am. Chem. Soc.* **118**, 11258 (1996).
- <sup>12</sup>L. A. Angel and K. M. Ervin, *J. Phys. Chem. A* **105**, 4042 (2001).
- <sup>13</sup>A. P. Bento and F. M. Bickelhaupt, *J. Org. Chem.* **73**, 7290 (2008).
- <sup>14</sup>P. Manikandan, J. Zhang, and W. L. Hase, *J. Phys. Chem. A* **116**, 3061 (2012).
- <sup>15</sup>H. Tachikawa and M. Igarashi, *Chem. Phys. Lett.* **303**, 81 (1999).
- <sup>16</sup>H. Tachikawa, M. Igarashi, and T. Ishibashi, *J. Phys. Chem. A* **106**, 10977 (2002).
- <sup>17</sup>I. Szabó, H. Telekes, and G. Czakó, *J. Chem. Phys.* **142**, 244301 (2015).
- <sup>18</sup>I. Szabó and G. Czakó, *J. Phys. Chem. A* **119**, 12231 (2015).
- <sup>19</sup>Y. Wang, H. Song, I. Szabó, G. Czakó, H. Guo, and M. Yang, *J. Phys. Chem. Lett.* **7**, 3322 (2016).
- <sup>20</sup>G. Czakó and J. M. Bowman, *J. Chem. Phys.* **131**, 244302 (2009).
- <sup>21</sup>G. Czakó, *J. Phys. Chem. A* **116**, 7467 (2012).
- <sup>22</sup>L. Bonnet and J. Espinosa-García, *J. Chem. Phys.* **133**, 164108 (2010).
- <sup>23</sup>W. L. Hase, *Encyclopedia of Computational Chemistry* (Wiley, New York, 1998), pp. 399–407.
- <sup>24</sup>J. Zhang, J. Xie, and W. L. Hase, *J. Phys. Chem. A* **119**, 12517 (2015).